

# Trade-off between reconstruction accuracy and physical validity in modeling turbomachinery PIV data by Physics-Informed CNN

---

Maryam Soltani<sup>1</sup>, Ghasem Akbari <sup>2,\*</sup>, and Nader Montazerin<sup>1</sup>

<sup>1</sup> Department of Mechanical Engineering, Amirkabir University of Technology, Tehran, Iran

<sup>2</sup> Department of Mechanical Engineering, Qazvin Branch, Islamic Azad University, Qazvin, Iran

\* Corresponding Author: g.akbari@qiau.ac.ir

## Abstract

Particle Image Velocimetry (PIV) data is a valuable asset in fluid mechanics. It is capable of visualizing flow structures even in complex physics scenarios, such as the flow at the exit of the rotor of a centrifugal fan. Machine learning is also a successful companion to PIV in order to increase data resolution or impute experimental gaps. While classical algorithms focus solely on replicating data using statistical metrics, the application of Physics Informed Neural Networks (PINN) contributes to both data reconstruction and adherence to governing equations. The present study utilizes a convolutional physics-informed auto-encoder to reproduce planar PIV fields in the gappy regions while also satisfying the mass conservation equation. It proposes a novel approach, which compromises experimental data reconstruction for compliance with physical restrictions. Simultaneously, it is aimed to ensure that the reconstruction error does not considerably deviate from the uncertainty band of the test data. Turbulence scale approximation is employed to set the relative weighting of the physical and non-physical terms in the loss function to ensure that both objectives are achieved. All steps are initially evaluated on a set of DNS data to demonstrate the general capability of the network. Finally, examination of the PIV data indicates that the proposed PINN auto-encoder can enhance reconstruction accuracy by about 28% and 29% in terms of mass conservation residual and velocity statistics, respectively, in expense of up to 5% increase in the number of vectors with reconstruction error higher than the uncertainty band of the PIV test data.

**Keywords:** physics-informed neural network, particle image velocimetry, mass conservation equation, loss function, direct numerical simulation

## I) Introduction

The world of fluid mechanics is faced with huge numerical and experimental data sets which makes it a perfect environment for the application of artificial intelligence tools. Extracting models from data in this field requires an expert who can manage the process and make crucial decisions [1]. The advancement of deep learning techniques has led to active research in applying them to the development of innovative approaches in the field of fluid mechanics [2,3].

Direct Numerical Solution (DNS) or high-order developed codes in Computational Fluid Dynamics (CFD) are accurate methods which are continuously developed for determining the state of the flow field. Results have shown that recent methods are not always cost-effective in terms of time and computational resources and require significant time and expense to obtain their solutions in large fields.

Implementation of experimental methods helps to identify complicated flow fields in which numerical approaches may fail due to enormous computational cost. Although experimental data is aligned with the physical reality of the phenomena, they may be contaminated with some noise and measurement uncertainty. Among various experimental methods, Particle Image Velocimetry (PIV) and its derivatives play a special role in spatio-temporal analysis of turbulent fields. Presence of some clustered or spot-wise missing data, induced by optical noise or inadequate seeding density, are challenges that should be resolved prior to further analysis. Different methods are employed for gappy velocity field reconstruction [4,5]. Classical methods for this reconstruction are statistical, but with the advancement of machine learning algorithms and deep learning, the idea of utilizing tools such as KNN (K-nearest-neighbor) or neural networks [6-8] for data imputation are proposed. A wide variety of deep learning methods, such as convolutional neural networks [9] and generative adversarial networks [10,11], are applied for the reconstruction of two-dimensional images and enhance the resolution of flow fields [12-14]. The common issue with these methods is that although they eventually report a numerical value for the velocity vector, the result only attempts to reproduce the experimental data without considering the physics of the problem.

Reconstructed fields from conventional methods for data completion, deviate from expected governing equations [15]. The governing physical equations of each problem could act as constraints to produce a more physical reconstruction. In 2019, the idea of physics-informed neural networks (PINN) was proposed [16]. PINN fundamentally leverages traditional neural networks and incorporates problem-dependent loss functions to address typical loss functions and also minimize deviations from the governing equations. This quickly sparked interest in applying these networks to different applications such as fluid mechanics for determining the velocity and pressure fields in conjunction with the Navier-Stokes equations [17]. This idea

incorporated information derived from physical laws and reduced the need for big data which is not always available [18].

PINN is numerously tested on DNS and CFD results to show its capabilities in applications where the data is ill-posed or incomplete [19-21]. The main power of PINNs lies in having robust loss functions that incorporate the physics of the problem. Various choices of such loss functions are made in different research studies [21-25]. In each of these studies, the loss function comprises of two components. The first component, termed the data-based term, aims to minimize the error between the predicted quantities and the available data. The second component, known as the physics-informed part, is formulated based on the inherent nature of the problem. Adding a regularization term to the loss function of a neural network involves introducing extra weights or hyper-parameters that need to be adjusted. While the significance of these parameters was previously unknown, and they were often chosen without explicit rationale in earlier works, recent studies have introduced diverse methodologies. These include analyzing the Hessian of the loss function [26], utilizing Neural Tangent Kernel Theory [27], and integrating the weighting hyper-parameters alongside trainable parameters [28].

The application of a physics-informed neural network to experimental fluid mechanics data, which might be sparse and subject to limitations imposed by the data acquisition procedure, is promising [29]. For instance, PINN is applied to experimental datasets from Tomographic Background Oriented Schlieren to infer velocity and pressure fields from temperature data [30]. This aids in reconstruction of dense velocity and pressure fields from sparse experimental data [31], as well as the reconstruction of velocity in one direction with the known velocity in another direction within a two-dimensional domain [22].

It is essential to note that, unlike the reconstruction of DNS data, in the application of PINN to experimental data, there are measurement errors in the collected data points. The contribution of this paper lies in its consideration of a trade-off, within the confines of experimental error, wherein reconstructed data may deviate from the original field but exhibits improved adherence to the governing equations. The present study defines a loss function that calculates the residuals of mass conservation equation and compares them with the residuals of the original data. The reconstruction completes the missing vector maps and also achieves better consistency with the mass conservation equation. This approach initially aims to perform reconstruction on artificially ill-posed DNS data and then applies the algorithm to the challenging problem of PIV data of a high-Reynolds turbulent flow at the rotor exit of a centrifugal fan. The goal is to show the trade-off between reconstructing the measured velocity field and complying with the mass conservation equation. The article further contributes by examining the impact of using weighted coefficients for different terms of the loss function on satisfying the mass conservation equation.

The rest of this article is organized as follows. In the next section, PIV data and the required preprocessing steps are introduced. It follows by the proposed methodology for the PINN and configuration of the network and loss function. The fourth section discusses the results for reconstruction of DNS and PIV data, providing a detailed evaluation of the influence of weighting coefficients on the accuracy of the proposed PINN network.

## II) Experimental data and pre-processing

### 2-1- PIV dataset

Stereoscopic PIV is used to measure velocity components at the rotor exit region of a forward-curved centrifugal fan. Data is acquired at an encoded position of the rotor. The experimental setup is shown in Figure 1 and includes the following components [32]:

- A 43-blade centrifugal fan constructed from galvanized plate
- A test setup and an outlet duct compatible with the ISO 5801 standard [33]
- A volute made of transparent Plexiglas to provide optical access to the test section
- An optical encoder to facilitate phase-locked encoding of rotor orientation
- A double-cavity Quantel Brilliant Nd-YAG laser equipped with an optical guide system that delivers the laser sheet to the test section
- Two FlowSense® 1600×1186-pixel double-frame CCD cameras
- SAFEX F2010 plus fog generator
- Dantec FlowMap® system for synchronization of laser, camera, and encoder actions.

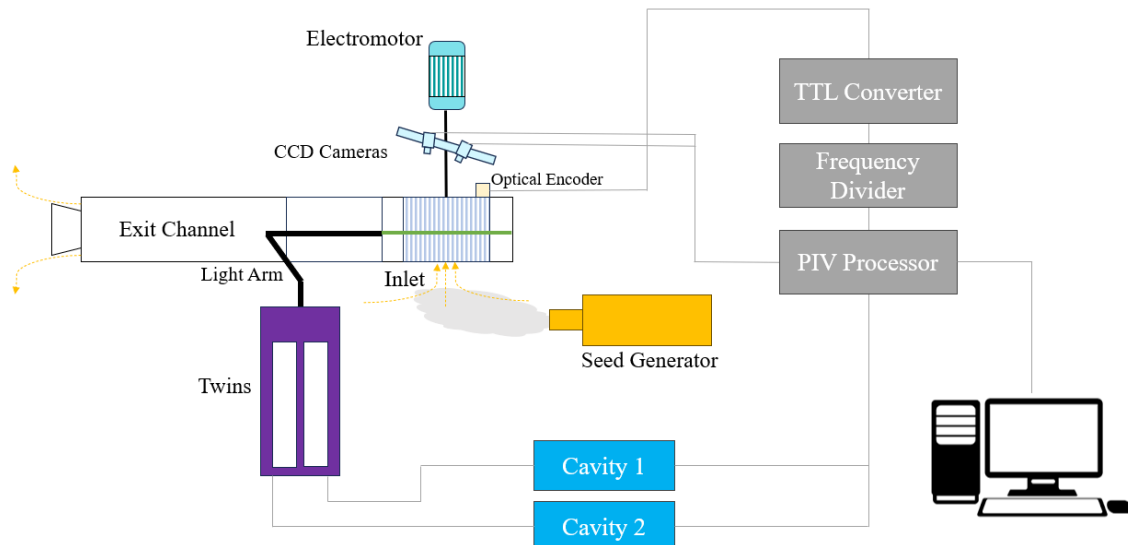


Figure 1 Schematic representation of the SPIV System

Velocity measurements are conducted in the upper rotor region at a plane perpendicular to the rotor axis, specifically at  $Z/B = 0.4$  [32]. Here,  $Z$  represents the axial coordinate, measured from the volute inlet, while  $B$  is the width of the volute (Figure 2(b)). The position of the field of views (FOVs) with respect to the rotor is illustrated in Figures 2(a) and 2(c). The selection measurement area involves the interaction between jet-wake-volute flow structures, which is divided into 10 FOVs with some overlaps in order to better resolve fine flow structures.

The number of snapshots for each FOV is 2500. During the data validation steps, some data is removed leading to generation of some gappy points in each snapshot. These invalidated data is due to lack of sufficient and homogeneous seeding, optical noises, loss-of-pair effect and complexity of the flow field. There is no general pattern for the location and the size of the gaps. In the present study, these gaps are classified into two groups. The first one are clustered gaps with more than one missing data in the neighborhood of each point, and the second one are individual gaps where the gappy point is surrounded from top, down, left and right neighbors by available data. In addition to these clustered or individual gaps (termed also as the original gaps), some artificial gaps are generated by a random algorithm. The purpose of these artificial gaps is to provide some test data for comparison of the model's reconstruction with the original velocity at those points.

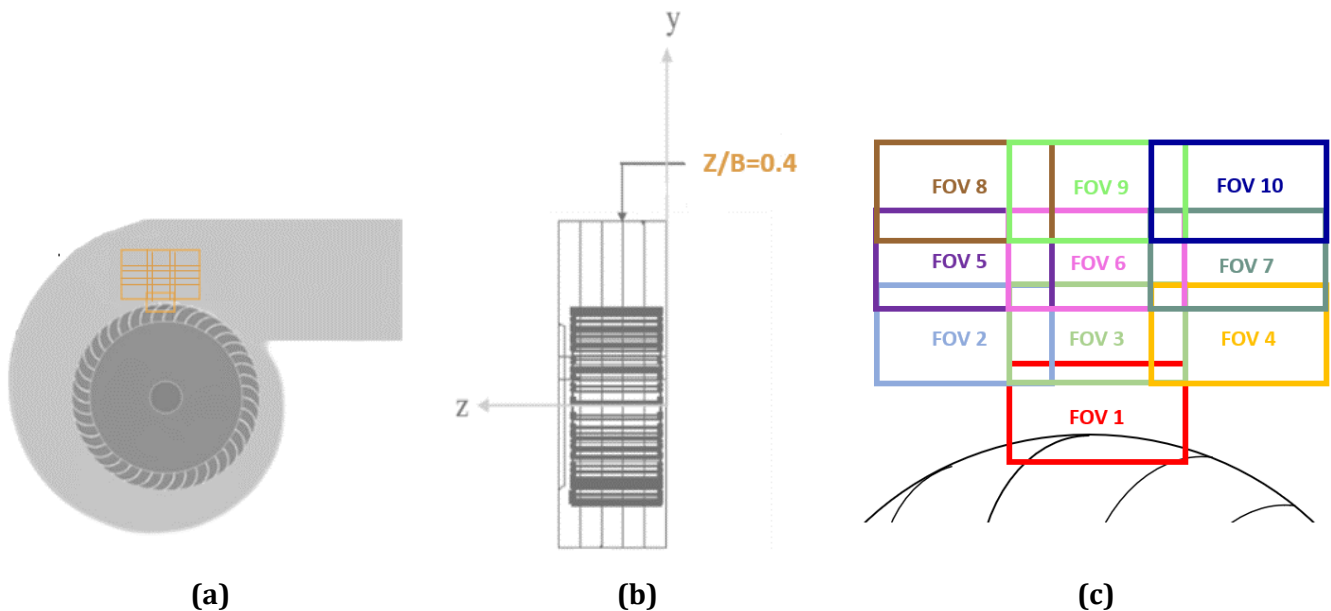


Figure 2 Sketch of centrifugal fan, and position of FOVs with respect to the Rotor: (a) front view of the rotor; (b) side view of the rotor; (c) position of FOVs.

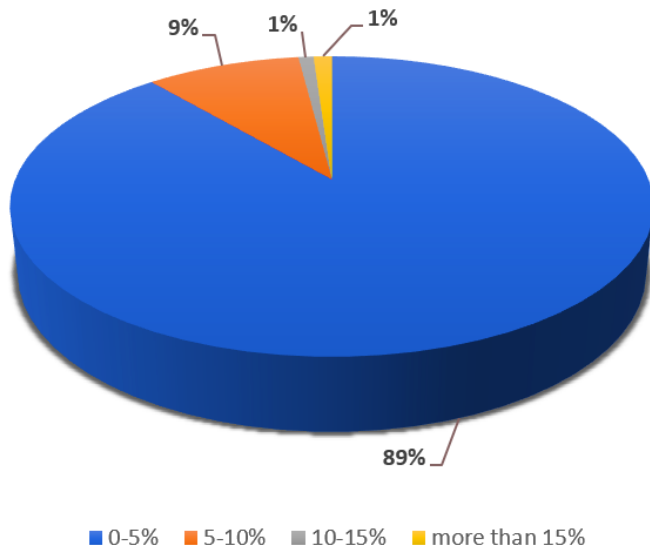


Figure 3 Percentage of PIV data gaps in FOV 2.

Figure 3 illustrates the percentage of gaps in snapshots of FOV2, and it indicates that 98% of the images have at least 90% valid data. Among all FOVs, the highest gap percentage belongs to FOV 1, due to some optical blockage with the rotor region. FOVs 5-9 which are farther away from the rotor, produce superior data quality due to more homogeneous seeding distribution and moderate velocity gradient.

## 2-2- Pre-processing

Preprocessing is applied to raw PIV data prior to velocity field reconstruction using PINN network. The resulting velocity field in some snapshots of the PIV experiments lacks a discernible pattern due to insufficient seeding particles. In the other words, the marginal difference between the values of velocity vectors, results in a field with no discernible gradient that could avoid identification of diverse flow patterns. Snapshots with the standard deviation of all normalized velocity vectors smaller than 1.5 are therefore identified and excluded from the dataset, before training the model.

Next, outliers in each snapshot are detected and replaced with gaps based on the z-score. This factor relies on the mean ( $\mu$ ) and standard deviation ( $\sigma$ ) of velocity field in each snapshot. If any of the velocity vectors is not within the range  $[\mu - 3\sigma, \mu + 3\sigma]$ , it is identified as an outlier and removed.

The next step is initial imputation of the original gaps with a classic statistical method, in order to provide a complete vector map as the input for the PINN network. This is because the convolution

kernel embedded in the PINN model cannot be applied to a sub-region containing missing values. Two-dimensional cubic spline is utilized to impute the data at the gap regions for each snapshot [15]. The PINN architecture then modifies this initialization, and makes the reconstruction more mature by implementing both data-driven and physics-informed metrics, as discussed in Section III.

The Next pre-processing step is normalization of the snapshot data. The global maximum and minimum velocities among all snapshots ( $V_{min}$  and  $V_{max}$ ) are used for normalization, as follows:

$$V^* = \frac{V_{original} - V_{min}}{V_{max} - V_{min}}. \quad (1)$$

### III) Methodology

PINNs are neural networks where both data and equations that are expected to govern that data are present in the loss function. Figure 4 provides a general overview of physics-informed neural networks where the selection and form of input can vary depending on the problem and the type of available data.

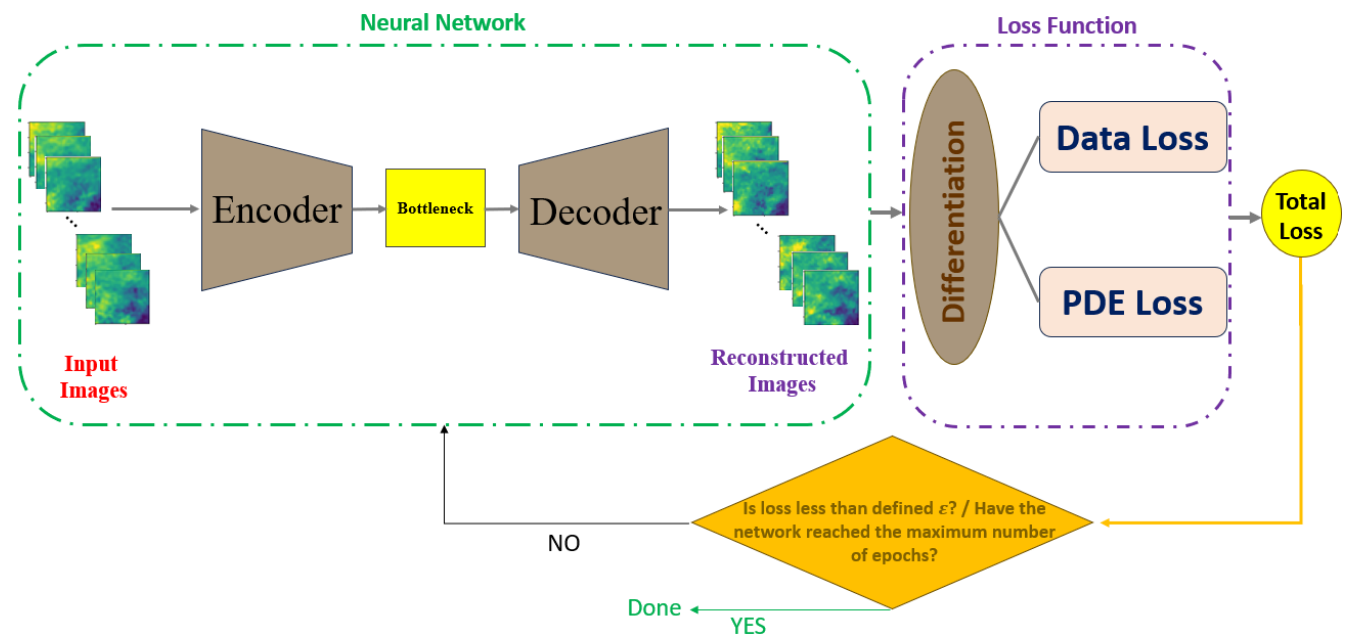


Figure 4: General flow of the physics-informed convolutional auto-encoder

### 3-1- Network architecture

Previous research on PINNs frequently selected spatial coordinates and time stamps as inputs for the network [30]. Such input is possible in the case of DNS or synthetic data, with sufficient spatio-temporal resolution. However, the PIV data is sparse, especially in the time domain, and therefore utilization of spatial coordinates and time as inputs does not allow automatic differentiation. In such circumstance, using velocity snapshots at different time stamps as individual input images and applying a convolutional network to identify spatial dependencies is the reasonable choice.

A convolutional encoder-decoder network is designed for this purpose, that receives a two-channel image (two feature maps corresponding to two in-plane velocity components) as the input and after imputation of the gaps, reconstructs the output vector map with the same resolution. Figure 4 schematically represents the encoder-decoder implementation in the current study. The details of the network is presented in Figure 5 for two-channel images with dimension  $36 \times 36$  vector maps for PIV data.

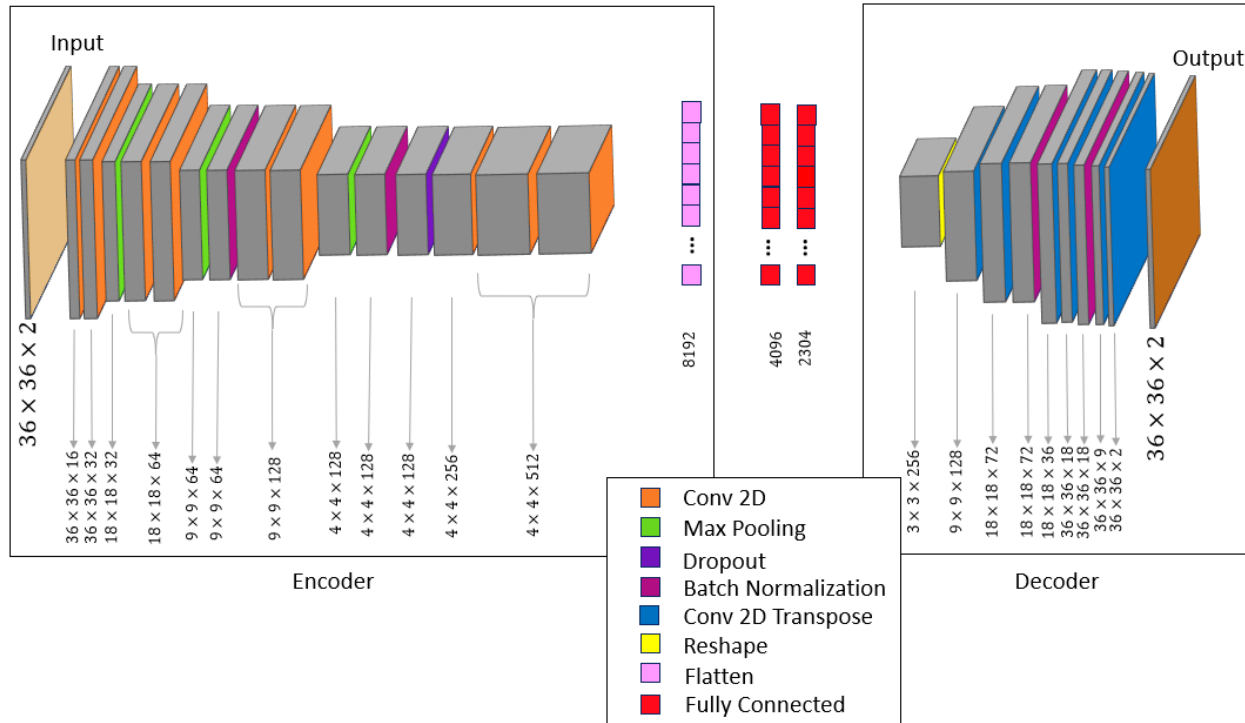


Figure 5 Architecture of the proposed physics-informed auto-encoder for PIV Data

The chosen network optimizer for the PINN model can significantly impact its performance and speed [34]. ADAM optimizer is used in the current research. At initial epochs, learning rate is constant, but an exponential decaying function is used to decrease learning rate in each epoch from initial value of 0.001. The network is designed based on the open-source platform TensorFlow v2.15.0, and computations are preformed through GPU of Google Colaboratory Pro.

### 3-2-Loss Function

A physics-informed neural network constrains the network to learn specific equations that encapsulate the physics inherent to the problem. The idea of adding physics-informed loss function to convolutional neural network for enhanced reconstruction is introduced to match the patterns with the physics of the flow [35,36]. The loss function in such networks includes terms that are dependent on the applied physics and other similar factors, thereby guiding predictions beyond mere replication of the original values. The classic data-based loss function evaluates the error between model prediction and actual values:

$$L_{data} = \frac{1}{N_{data}} \left( \sum_{j=1}^{N_{data}} |U_{model} - U_{actual}|^2 \right) \quad (2)$$

where  $N_{data}$  is the number of evaluation samples and  $U$  represents the velocity vector. For the physics-based loss function, various equations can be employed depending on the nature of the problem. Generally, it can be formulated with a residual that is calculated based on the physical equation ( $R$ ), as follows:

$$L_{physical} = \frac{1}{N_{ph}} \sum_{j=1}^{N_{ph}} |R_{model} - R_{actual}|^2 \quad (3)$$

where  $R_{model}$  and  $R_{actual}$  are the residuals evaluated based on the model prediction and actual data, respectively.  $N_{ph}$  represents the number of samples participating in calculation of the residual. There is no requirement for the same value of  $N_{ph}$  and  $N_{data}$ . The following weighted sum can be applied to adjust the impact of data-based and physics-based loss terms:

$$L_{tot} = \alpha_{data} L_{data} + \alpha_{physical} L_{physical} \quad (4)$$

where the parameters  $\alpha_{data}$  and  $\alpha_{physical}$  are weight coefficients.

A novelty of this article lies in examining the trade-off between the physics-based and data-based loss terms. In other words, whether it is possible to improve both of these aspects in the empirical data or if there is a compromise between them, much like a trade-off, where data-based term can vary within the experimental error band in order to bring the predicted data closer to the governing equations. The proposed methodology for calculating the physics-based loss and the weight coefficients is discussed in the following.

### 3-2-1- Physics-based loss function

Mass conservation law is considered as the physical constraint for the PINN model in the present study. Generally, the conservation of mass equation is expressed as follows:

$$\frac{\partial u}{\partial x} + \frac{\partial v}{\partial y} + \frac{\partial w}{\partial z} = 0 \quad (5)$$

where  $u$  and  $v$  are the in-plane velocity components and  $w$  is the out-of-plane component. If the flow is two-dimensional (like the DNS dataset utilized in section 4-1),  $\frac{\partial u}{\partial x} + \frac{\partial v}{\partial y} = 0$  reflects the mass conservation law perfectly. However, for a three-dimensional data (like the experimental dataset of the present study),  $\frac{\partial w}{\partial z} \neq 0$ . For the single-plane PIV data,  $\frac{\partial w}{\partial z}$  can not be evaluated, and just the in-plane components of velocity gradient are calculated. Therefore, in order to implement the mass conservation law in the loss function, we considered reconstruction of the out-of-plane component based on the available in-plane components, i.e.  $\frac{\partial w}{\partial z} = -\left(\frac{\partial u}{\partial x} + \frac{\partial v}{\partial y}\right)$ , and therefore utilized the term  $\frac{\partial u}{\partial x} + \frac{\partial v}{\partial y}$  as the representative (residual) of the mass conservation law in the physical loss, as follows:

$$L_{physical} = \frac{1}{N_{ph}} \sum_{j=1}^{N_{ph}} \left| \left( \frac{\partial u}{\partial x} + \frac{\partial v}{\partial y} \right)_{model} - \left( \frac{\partial u}{\partial x} + \frac{\partial v}{\partial y} \right)_{actual} \right|^2 \quad (6)$$

The derivatives in equation (6) are calculated by second-order central difference scheme [37].

### 3-2-2- Data-based loss function

The initial idea for defining the data-based loss function consisted of five terms:

$$L_{data} = \frac{1}{N_d} \left( \sum_{j=1}^{N_d} |(u)_{model} - (u)_{actual}|^2 + \sum_{j=1}^{N_d} |(v)_{model} - (v)_{actual}|^2 \right. \\ \left. + \sum_{j=1}^{N_d} \left| \left( \frac{\partial u}{\partial x} \right)_{model} - \left( \frac{\partial u}{\partial x} \right)_{actual} \right|^2 \right. \\ \left. + \sum_{j=1}^{N_d} \left| \left( \frac{\partial v}{\partial y} \right)_{model} - \left( \frac{\partial v}{\partial y} \right)_{actual} \right|^2 + \sum_{j=1}^{N_d} \left| \left( \frac{\partial v}{\partial x} - \frac{\partial u}{\partial y} \right)_{model} \right. \right. \\ \left. \left. - \left( \frac{\partial v}{\partial x} - \frac{\partial u}{\partial y} \right)_{actual} \right|^2 \right) \quad (7)$$

The first two terms in the right-hand-side of Equation (7) pertain to the velocity prediction error in horizontal and vertical directions. The third and fourth terms evaluate the predicted in-plane velocity gradients with the actual values, and the last term assesses reconstruction of the out-of-plane vorticity component (the only calculable component for a single-plane PIV data). The inclusion of the last three derivative-based terms significantly amplifies numerical errors in the loss function. This in turn, slows down convergence, necessitates utilization of more epochs, and increases the risk of overfitting. So, the final form of data-based loss function applied in the present study is as follows:

$$L_{data} = \frac{1}{N_d} \left( \sum_{j=1}^{N_d} |(u)_{model} - (u)_{actual}|^2 + \sum_{j=1}^{N_d} |(v)_{model} - (v)_{actual}|^2 \right) \quad (8)$$

The contribution of  $L_{data}$  and  $L_{physical}$  obtained from equations (6) and (8) can be adjusted using the weighting factors, based on equation (4), to calculate the total loss.

Another important aspect is the determination of number of locations that participate in each term of the loss function, i.e.  $N_{ph}$  and  $N_{data}$ . Calculation of the derivatives in the physical term at each point requires velocity data at the four neighbors of that point. Evaluation of the generated artificial gaps indicated that the number of points satisfying such condition was not sufficient to obtain a stable loss. So, for the physical term, every point in the field with all four neighbors available, is employed in the calculation of loss function. On the other hand, the data-based loss term does not require knowledge of the neighbor data, and it is only calculated at the artificial gaps.

### 3-2-3- Weight coefficients

The parameters  $\alpha_{data}$  and  $\alpha_{physical}$  in Equation (4) determine the influence of different terms in the loss function, which has not been explicitly discussed in initial research on physics-informed neural networks [16]. Although in some studies, changes in these weights significantly changed the outcomes, but no specific rationale for selecting final values was put forward [29-31]. The importance of these weighting coefficients is crucial for accelerating network convergence and also for providing a logical definition of the relationship between different terms. Ideas for how to select or update these coefficients are suggested in some papers, but these ideas lack a clear physical connection to the type of flow [27,38]. Although these methods lack a physics-based justification, they show significant improvements compared to cases where the loss function is considered with equal weighting coefficients. From a different perspective, Leoni et al. [25] proposed an approach based on turbulence scale analysis to approximate the order of weight coefficients. The advantage of this method, which is also applied in the present study, is that it pays attention to physical nature and turbulence characteristics of the flow.

The following estimation is suggested for the ratio of weight coefficients ( $\gamma$ ), which is based on the definition of total loss (Equation (4)) assuming the same order of magnitude for data-based and physics-based terms:

$$\gamma = \frac{\alpha_{data}}{\alpha_{physical}} \sim \frac{L_{physical}}{L_{data}} \quad (9)$$

Based on Equations (6) and (8),  $L_{physical} \sim (\frac{\partial u}{\partial x})^2$  and  $L_{data} \sim u^2$ . Since the velocity field is normalized, the order of  $u$ , and therefore  $L_{data}$  is unity, leading to  $\gamma \sim (\frac{\partial u}{\partial x})^2$  from Equation (9). The order of magnitude for the velocity gradient is estimated for a turbulent flow with turbulence dissipation  $\varepsilon$  and length scale  $l$  as follows [25]:

$$\frac{\partial u}{\partial x} = \varepsilon^{1/3} l^{-2/3}. \quad (10)$$

The largest value of this estimate happens at the smallest scale of turbulent flow, i.e. the Kolmogorov length scale  $\eta \sim \nu^{3/4} \varepsilon^{-1/4}$ . So, equation (10) is expressed as follows:

$$\frac{\partial u}{\partial x} = \varepsilon^{1/2} \nu^{-1/2} \quad (11)$$

According to PIV data of the present study and using equation (11),  $\frac{\partial u}{\partial x}$  is estimated to be about 10, and therefore the ratio of weight coefficients is estimated to be about 100.

### 3-3- Network Assessment

The loss function should align with a suitable metric for evaluating network performance. In the present study, evaluation is done by plotting predicted values for the gaps vs. the original values expected in a line graph, with the same scales for the horizontal and vertical axes. Accordingly, a 45-degree line will be the reference line for network evaluation and there is no error in the reconstruction for data perfectly aligned with this reference line. A set of unseen snapshots is used for assessment. The mean absolute error ( $MAE$ ) between prediction and target values (average vertical distance between cluster of points and the reference 45-degree line) is considered as the measure of error in order to enable comparisons across different snapshots:

$$MAE(\phi) = \frac{1}{N} \sum_{i=1}^N |\phi_{predicted} - \phi_{target}| \quad (12)$$

where  $\phi$  represents each of the target quantities for evaluation, including horizontal and vertical velocity components ( $u$  and  $v$ ) and mass conservation residual ( $MC$ ), defined as follows:

$$MC = \frac{\partial u}{\partial x} + \frac{\partial v}{\partial y} \quad (13)$$

## IV) Results and Discussion

The idea of establishing a trade-off between reproducing the exact velocity pattern of a flow, or missing the original data within its experimental error band but complying with the mass conservation law is examined in the present article with two data sets. Initially, a DNS dataset is used to allow evaluation of the network on a data with no gaps and no uncertainties. It is expected that addition of the mass conservation equation (physical term) to the loss function, would reduce errors and help velocity field reconstruction. Then a PIV dataset with an estimated uncertainty level is used to evaluate the model performance. The addition of the physical term in this case could improve data reproduction or bring about a trade-off between data deviation from its original values for improved adherence to the governing equation.

### 4-1-DNS data reconstruction

DNS data is the result of direct simulation of the Naiver-Stokes equations (including mass conservation law) and follows them strictly. There is no error band (except for the very tiny computational errors) to allow for a trade-off towards improved adherence to the mass conservation law. It is therefore expected that the addition of the mass conservation equation to the loss function should bring the reconstructed pattern closer to the original data and reduce the reconstruction error.

A set of 150 time-resolved snapshots from a 2D DNS data around a cylinder [39] is used as the test case. DNS data needs a minimal pre-processing in comparison with the PIV data due to the absence of outliers, high quality of velocity data and availability of all data points. About 75% of the data is used for training and the remaining for the test procedure.

Velocity values in all snapshots are initially normalized and random vector maps in each image are transformed into individual or cluster gaps (about 25% of data at each snapshot is transformed to gaps). Gap positions are different for various snapshots, but they are kept the same at different executions. The next step is the imputation of each removed data point using cubic spline method. This is done just to imitate what shall happen to the experimental gappy points in the PIV data in the next section. The images are then fed into the network to undergo training procedure.

Mutual impact of physical and data-based terms of the loss function on each other are now studied. The results of reconstruction are examined for similar conditions in six cases, using a data-based convolutional neural network and five physics-based convolutional neural networks. Figure 6 shows the variations of the network loss with the number of epochs for both physics-based and data-based terms. The two loss terms do not converge with similar patterns. The

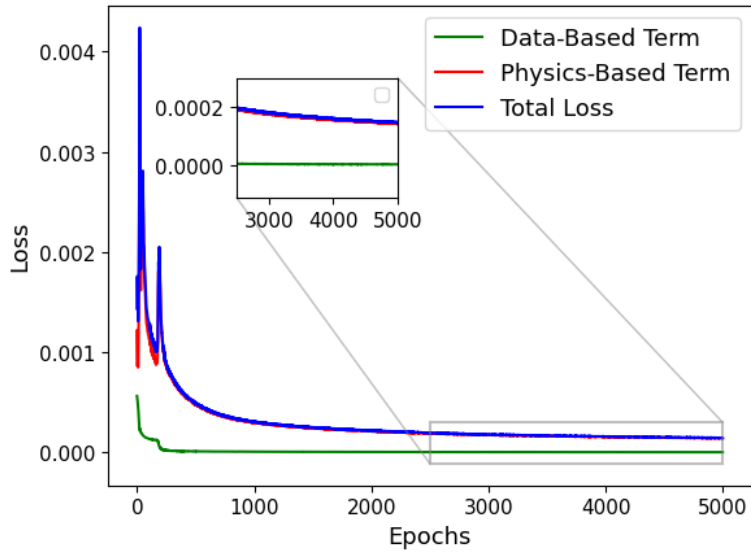


Figure 6 Convergence of the different loss terms during the training of PINN for the DNS data ( $\alpha_p = 1, \alpha_d = 1$ ).

physical term dominates the loss function, due to amplification of errors in numerical calculation of derivatives. The data-based loss is far more well behaved at early epochs and converges when the physical term still shows large fluctuations. Figure A1 in the appendix presents samples of the reconstructed images.

Velocity field reconstruction is evaluated for six different configurations of  $(\alpha_p, \alpha_d)$  to examine the contribution of physical and data-based terms of the loss function on the accuracy of the model. This includes a pure data-based CNN ( $\alpha_p = 0, \alpha_d = 1$ ), termed as the baseline configuration, and five physics-based CNNs with different weight configurations, namely  $(\alpha_p = 0.01, \alpha_d = 1)$ ,  $(\alpha_p = 0.1, \alpha_d = 1)$ ,  $(\alpha_p = 1, \alpha_d = 1)$ ,  $(\alpha_p = 1, \alpha_d = 10)$  and  $(\alpha_p = 1, \alpha_d = 100)$ . Figure 7 presents the scatter plot of prediction-target values for velocity components and mass conservation residual for these six configurations. Each point represents a snapshot and if any of these points is completely positioned on the line, it means on average perfect reconstruction of that snapshot. Additionally, Table 1 presents *MAE* calculated for these quantities, as well as the relative change of *MAE* ( $\epsilon$ ) for each physics-based configuration with respect to the baseline (pure CNN) configuration, defined as follows:

$$\epsilon(\phi) = 100 \frac{MAE_{baseline}(\phi) - MAE_{physics-based}(\phi)}{MAE_{baseline}(\phi)} \quad (14)$$

For each target quantity  $\phi$ , positive value of  $\epsilon$  indicates superior accuracy of physics-based network compared to the baseline network, and vice versa.

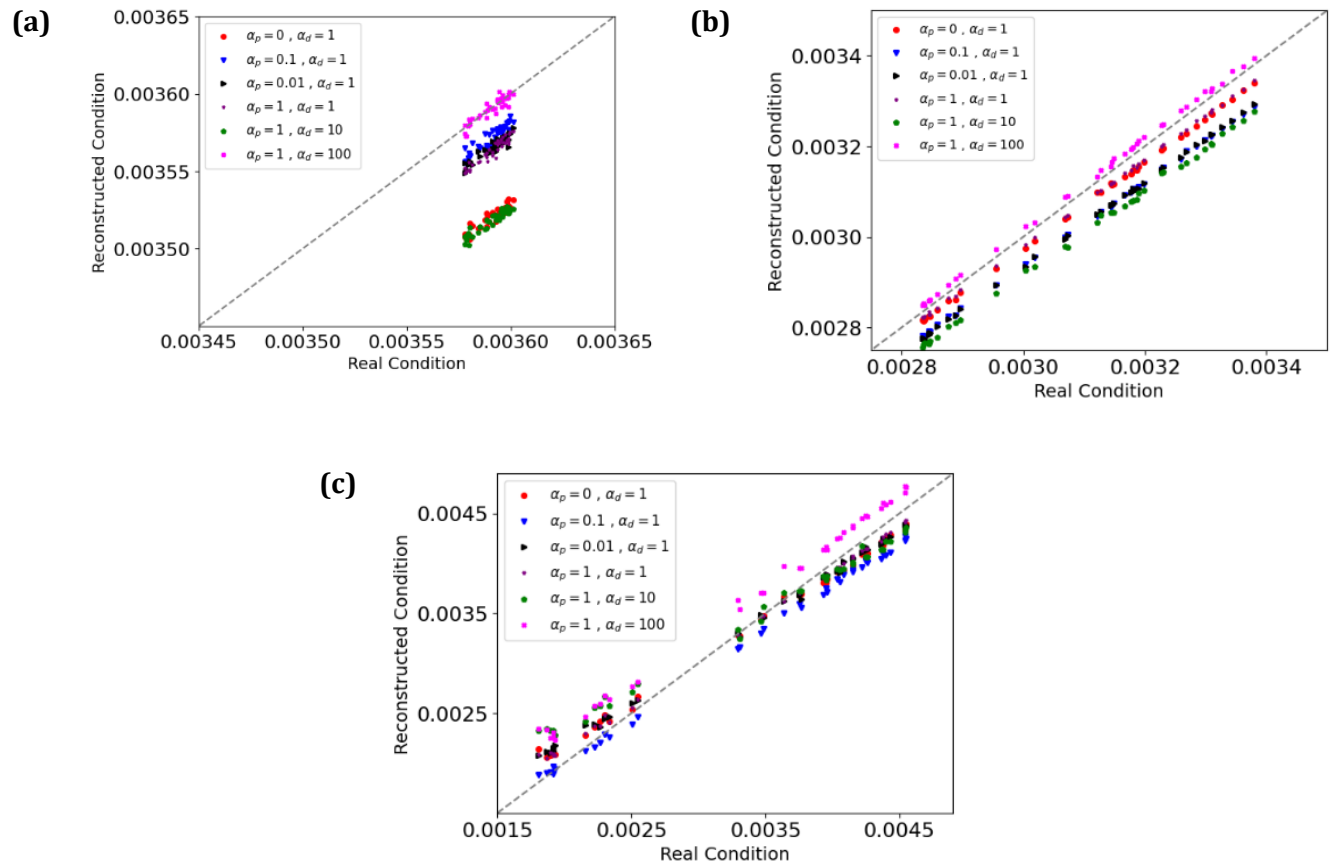


Figure 7 Comparison of model prediction and actual values for reconstruction of DNS data, in terms of: (a) horizontal velocity component; (b) vertical velocity component; (c) mass conservation residual.

Table 1 Accuracy of different physics-based configurations compared to the baseline network for the DNS data

Case	$\alpha_p$	$\alpha_d$	Horizontal velocity		Vertical velocity		Mass conservation residual	
			$MAE(u) \times 10^5$	$\epsilon(\phi) \%$	$MAE(v) \times 10^5$	$\epsilon(v) \%$	$MAE(MC) \times 10^5$	$\epsilon(MC) \%$
1 (baseline)	0	1	7.07	—	3.04	—	13.20	—
2	0.1	1	1.89	73.26	7.20	-136.84	16.75	-26.89
3	0.01	1	2.58	63.50	7.26	-138.81	12.67	4.01
4	1	1	2.76	60.96	2.42	20.39	<b>10.33</b>	<b>21.74</b>
5	1	10	7.30	-3.25	9.05	-197.69	20.31	-53.86
6	1	100	<b>0.24</b>	<b>96.60</b>	<b>1.75</b>	<b>42.43</b>	26.69	-102.19

Figure 7 indicates the importance of selecting optimal weight coefficients for the network accuracy in terms of velocity or mass conservation metrics. The cluster of points for horizontal velocity reconstruction is mostly distinct from the 45-degree line, while the velocity reconstruction in the vertical direction and the mass conservation residual could in some cases be very close to the target values, depending on the selected set of coefficients. Positive values of  $\epsilon$  in Table 1 indicate the superiority level of the physics-informed network as compared to the baseline model. It is shown in Table 1 that inclusion of physical term in the loss function in most of cases (expect case 5) enhances reconstruction of the horizontal velocity component, which is the dominant component of velocity field for the DNS data. Case 6 ( $\alpha_p = 1, \alpha_d = 100$ ) leads to the best accuracy, with respect to the baseline results, in terms of both velocity components. The relative enhancement is 96.6% and 42.43% for the horizontal and vertical components, respectively. However, this is not necessarily aligned with improvement of mass conservation residual. An opposite trend is observed in terms of mass conservation residual (by 102.19% relative reduction with respect to the baseline model). Overall, considering both velocity components and mass conservation residual metrics, case 4 ( $\alpha_p = 1, \alpha_d = 1$ ) results in the best performance. This case is a win-win compromise, such that 21.74% enhancement in *MC* reconstruction accompanies by 60.96% and 20.39% improvement of reproduction for the velocity components.

Figure 7 and Table 1 also indicate that the quality of velocity field reconstruction does not solely depend on the ratio of  $\alpha_p$  to  $\alpha_d$ , while it is also dependent to the value of these coefficients as well. For instance, if case 6 with  $\alpha_p/\alpha_d = 0.01$ , is compared with case 3 with the same weights ratio, the former shows a better accuracy in terms of mass conservation residual, but a lower accuracy for both velocity components.

## 4-2- PIV Data Reconstruction

The present section examines PINN model performance in reconstruction of the PIV data acquired at the rotor exit region of a centrifugal turbomachine. The images in this dataset all have  $36 \times 36$  vector maps, while some points in each snapshot have missing velocities. Figure 8 illustrates histograms of four sample snapshots after outlier detection. Some of the velocity data (less than 1%) are outliers and should be removed in the pre-processing step. 90% of the normalized dataset is used for the training phase, and the rest for the test phase. The subsequent pre-processing steps for the network's input are as presented in section 2-2, which are graphically illustrated in Figure 9 for one randomly selected snapshot. Fig. A2 in the appendix shows samples of reconstructed PIV data.

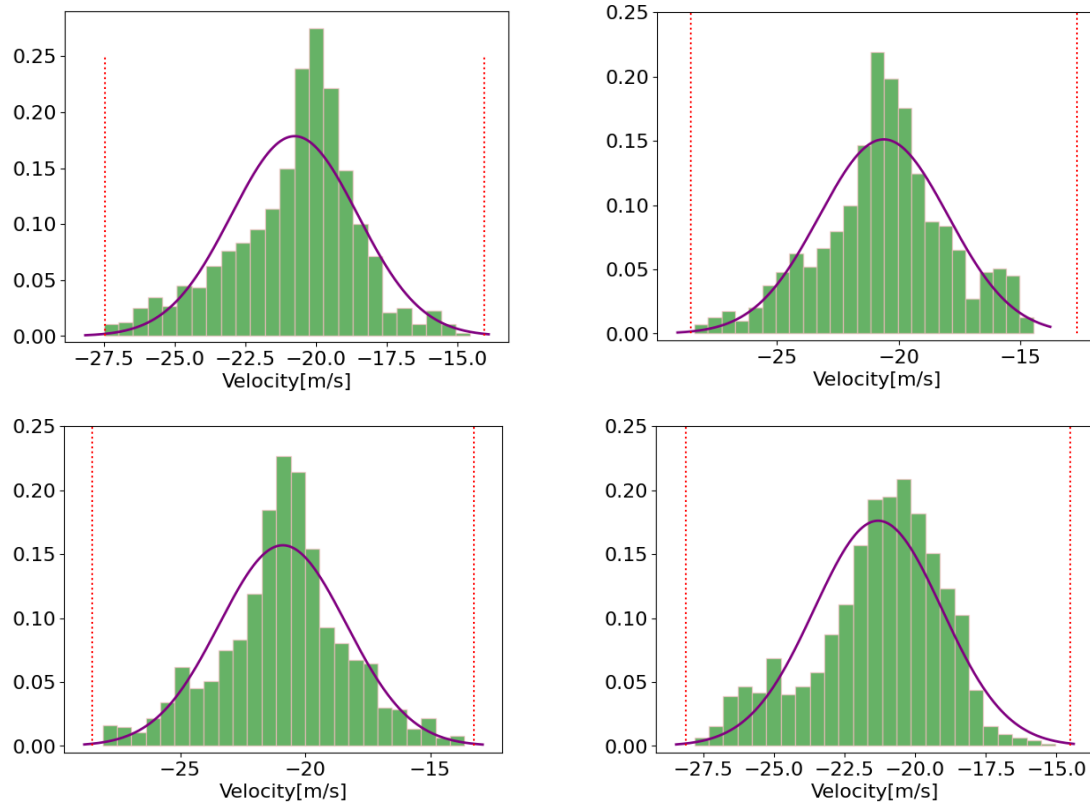


Figure 8 Histogram of instantaneous velocity for 4 random PIV snapshots after outlier removal.  
Red dash lines show the proposed band by z-score criteria.

It was shown in the previous section that a loss function with a mass conservation term, with suitable configuration of weight coefficients, could both improve DNS data reconstruction and make reconstructed data comply with the mass conservation equation. This was expected since the physical term was also used beforehand in the simulation step as a conservation law. To examine the same problem for the PIV data, Figure 10 illustrates the results of the physics-informed network for five different configurations of weight coefficients (same as section 4-1) and also compares them with the baseline pure CNN network. Table 2 presents the statistical evaluation of these results in terms of  $MAE$  and  $\epsilon$ . The point in Table 2 is the general enhancement of reconstruction accuracy for the horizontal velocity (as the dominant velocity component in this PIV data), in addition to improvement of mass conservation residual. The only exception is case 5 in which horizontal velocity component is almost unaffected by PINN model ( $\epsilon_u = -0.52\%$ ). So, for such cases, in addition to better conformity of the model to the physical principles, the statistical accuracy of velocity field reconstruction is also improved.

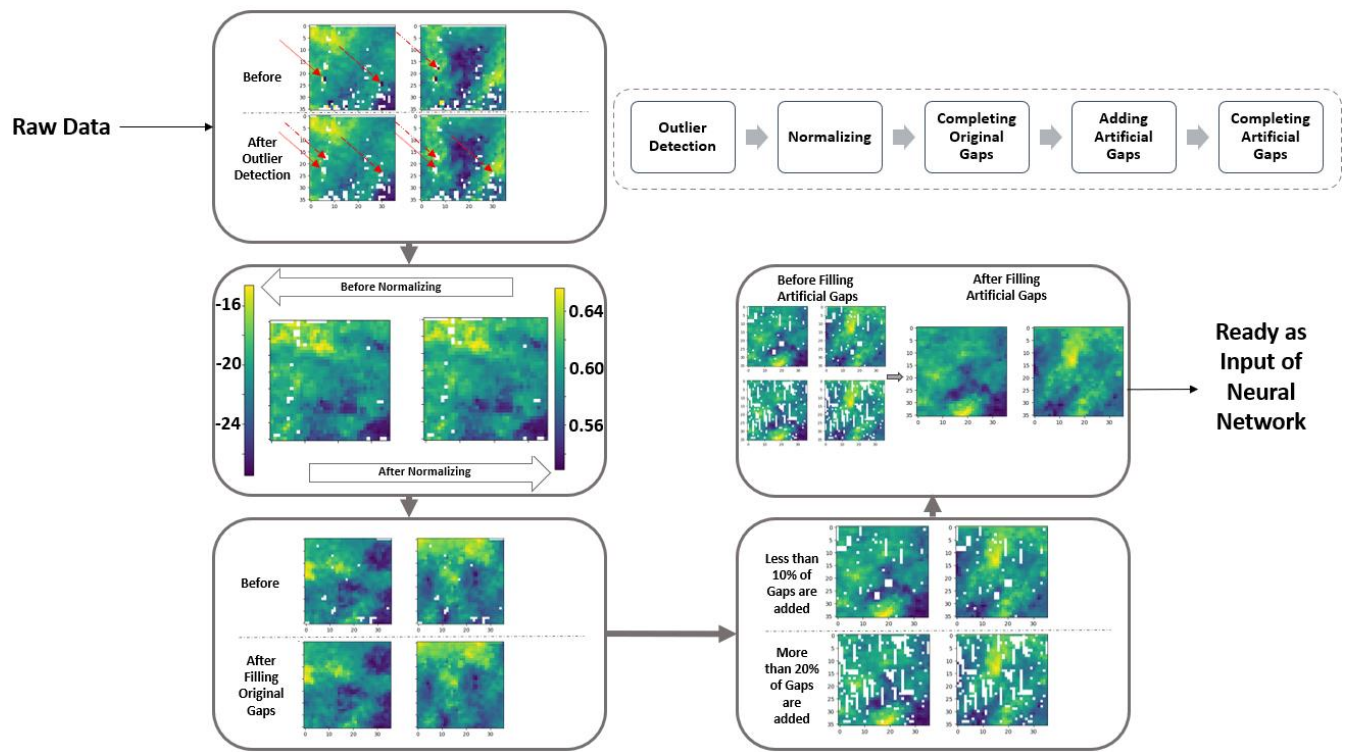


Figure 9 Representation of pre-processing steps for the PIV Data.

Unlike the DNS data, the PIV data is less sensitive to weighting coefficients, but derivatives are more difficult to reconstruct or optimize due to experimental noise and uncertainties. Table 2 shows that the worst case in terms of mass conservation metric is when the physical term is not present in the loss function (the baseline model). This does not mean that as weight coefficient corresponding to the physical term increases, reconstruction of mass conservation residual also enhances. Among the five configurations of weight coefficients, case 6 with the lowest weights ratio of  $\alpha_p/\alpha_d = 1/100$  leads to the highest performance in terms of mass conservation and both velocity components. This ratio was calculated based on turbulence scale analysis too. A larger weight ratio highlights the physical term but due to amplification of experimental uncertainties in the derivative operation, such augmented contribution in the physical term does not necessarily enhance the reconstruction accuracy. This issue is also shown in Figure 11-c, that despite some displacement of cluster of points toward the 45-degree line, it is not possible to strictly satisfy the mass conservation law, due to such uncertainty amplifications. Consequently, there is a trade-off between implementation of physical loss and obtaining some enhancement in the reconstruction accuracy on the one side, and deterioration of the results by excessive highlight of the physical term on the other side.

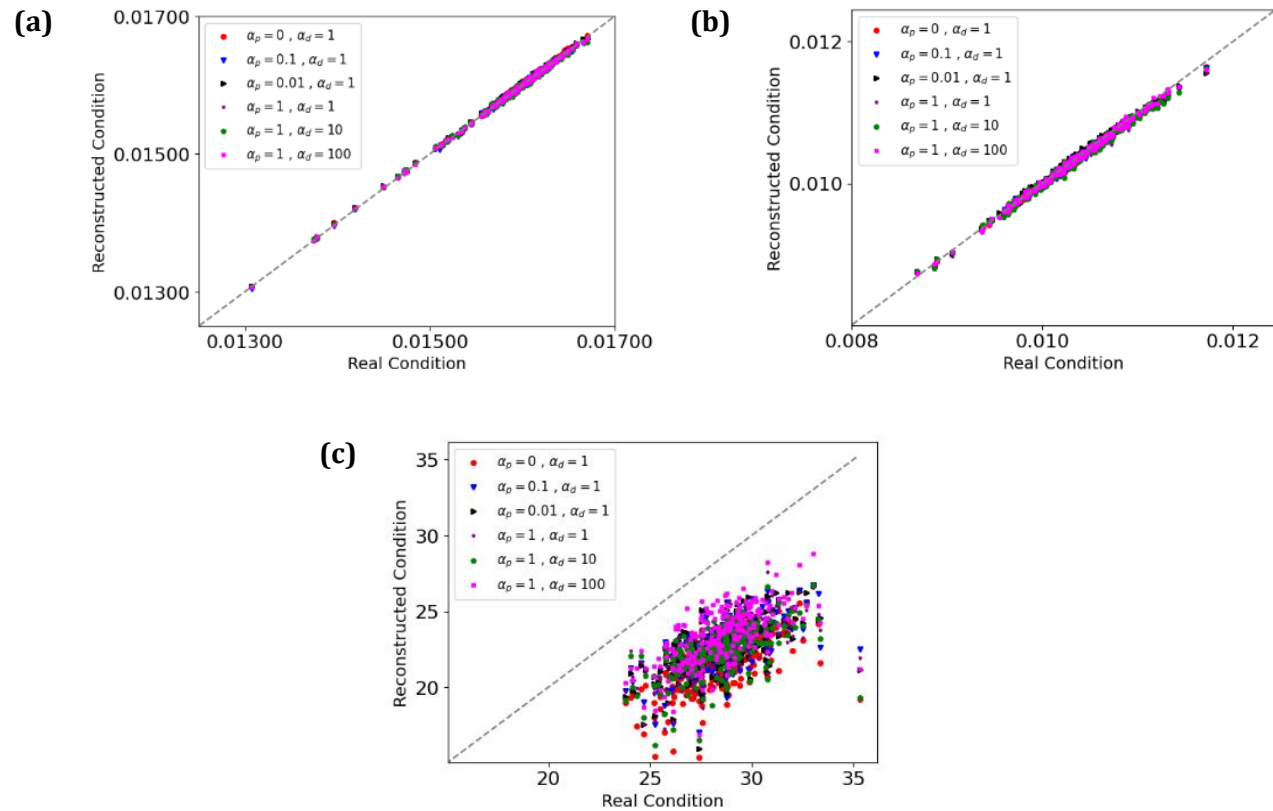


Figure 10 Comparison of model prediction and actual values for reconstruction of PIV data, in terms of: (a) horizontal velocity component; (b) vertical velocity component; (c) mass conservation residual.

Table 2 Accuracy of different physics-based configurations compared to the baseline network for the PIV data

Case	$\alpha_p$	$\alpha_d$	Horizontal velocity		Vertical velocity		Mass conservation residual	
			$MAE(u) \times 10^5$	$\epsilon(\phi) \%$	$MAE(v) \times 10^5$	$\epsilon(v) \%$	$MAE(MC)$	$\epsilon(MC) \%$
1 (baseline)	0	1	1.92	—	2.55	—	7.05	—
2	0.1	1	1.59	17.18	3.20	-25.49	5.86	16.87
3	0.01	1	1.64	14.58	2.83	-10.98	5.89	16.45
4	1	1	1.62	15.62	3.59	-40.78	6.00	14.89
5	1	10	1.93	-0.52	3.96	-55.29	6.09	13.61
6	1	100	<b>1.37</b>	<b>28.64</b>	<b>2.52</b>	<b>1.17</b>	<b>5.09</b>	<b>27.80</b>

Although based on the uncertainty level of any other data, a closer match of mass conservation residuals with the 45-degree line might be possible by tuning  $\alpha_p$  and  $\alpha_d$ , this should be only attempted if any further participation of the physical term would not cross the uncertainty limit

of the velocity components. This issue is studied for the current PIV data and the reconstruction error is compared with the experimental uncertainty. There are two types of uncertainties in the experimental data, namely random errors and bias errors. Random errors are due to non-systematic measurement characteristics, such as optical noise, and they can be reduced by repeating the experiment with stronger emphasis on the standard requirements and procedures. Bias errors are systematic and predictable. Errors due to particle lag effect, light refraction and displacement estimation are the most important bias errors in PIV measurement, which can be controlled by suitable selection and utilization of PIV components. The maximum bias error for the in-plane velocity components in the current data was estimated to be 1.5% [40].

Figure 11 presents the histogram of velocity components reconstruction based on three different configurations of weight coefficients, i.e. cases 3 and 6, and the baseline (pure data-based) model. It also compares the distribution with the normalized error band (red dashed line) deduced from experimental uncertainty. Quantitatively, Table 3 represents percentage of reconstructed vectors with error less than the experimental uncertainty, for each case in Figure 11. Table 3 indicates that the baseline model, reconstructs the PIV data such that about 90% of horizontal velocity components are within the experimental error band. By adding the physics-based term to the loss function, this percentage just reduces about 4-5%, while at the same time Table 2 reveals about 16% and 28% improvement in the reconstruction results of cases 3 and 6, in terms of the mass conservation residual, and about 15% and 29% enhancement in terms of horizontal velocity component. Therefore, limited excess from the uncertainty band in velocity reconstruction could enhance the reconstruction results, both in terms of data-based and physics-based metrics. However, this should be carried out by controlled adjustment of the contribution of physical term, because this derivative-based component can significantly amplify numerical instabilities resulting in deterioration of model convergence and accuracy.

## V) Conclusion

The performance of physics-informed convolutional neural networks for the reconstruction of experimental phase-resolved data around a centrifugal turbomachine was investigated. The objective was to impute PIV data in the gappy regions such that they comply with a trade-off between the mass conservation equation and the conventional velocity field statistics. This was carried out by proposing a convolutional auto-encoder network with a physics-based loss function relying on mass conservation residual.

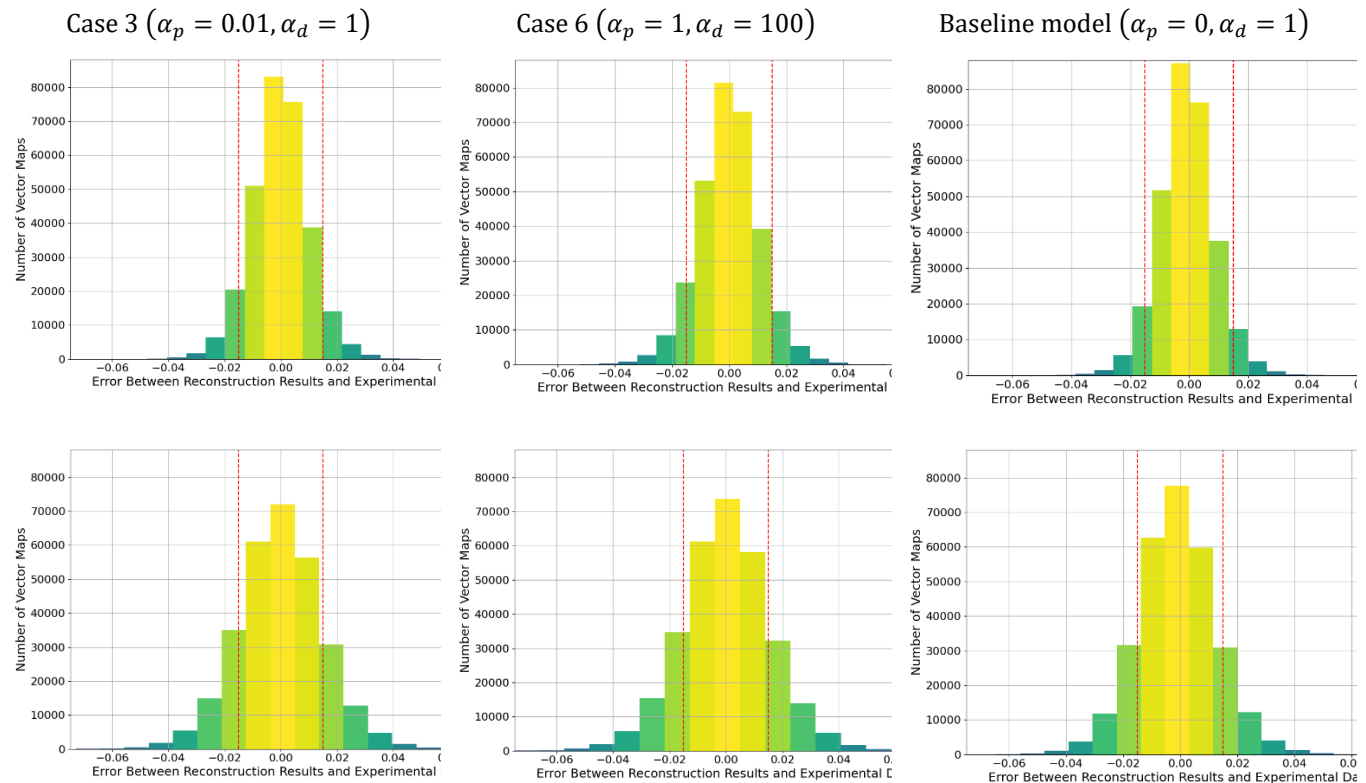


Figure 11 Histogram of reconstruction errors for horizontal (top row) and vertical (bottom row) components of velocity, based on three different configurations of weight coefficients

Table 3 Percentage of reconstructed vectors with error less than the experimental uncertainty.

	Case 3 ( $\alpha_p = 0.01, \alpha_d = 1$ )	Case 6 ( $\alpha_p = 1, \alpha_d = 100$ )	Baseline model ( $\alpha_p = 0, \alpha_d = 1$ )
Horizontal velocity	86.62%	85.28%	89.74%
Vertical velocity	70.28%	68.44%	74.66%

DNS data of flow past a cylinder, as a flawless, accurate and physics-based data, was initially used to study the performance of the proposed PINN model. The model was then evaluated based on the planar PIV data, to further investigate its performance on a more challenging dataset involving experimental uncertainties. The results for both DNS and PIV datasets demonstrated that optimal incorporation of a physics-based equation into the loss function not only improves the overall agreement with the mass conservation equation, but also results in more accurate reconstruction of velocities.

The impact of weight coefficients for the physical and non-physical terms in the loss function was examined based on the accuracy of reconstructed data. Reconstructed data exhibited a noticeable movement towards satisfying mass conservation equation after adjusting weight coefficients in the DNS data. However, for the PIV data, although the addition of physical terms in the loss function proved to be beneficial, there was still a considerable gap to achieve complete reproduction of the physical equations. One possible reason is the existence of experimental uncertainty in the measured velocity field, which can be considerably amplified by implementation of derivative-based physical principles (like mass conservation law) to the loss function. Another reason could be the unavailable velocity gradients in the out-of-plane direction, which enforce a two-dimensional mass conservation residual to the loss function. Furthermore, the nature of PIV data in a turbomachine involves complex patterns, making network convergence significantly more challenging as compared with the DNS data of flow past a cylinder. Nevertheless, the results indicated that by controlled adjustment of weight coefficients, the network managed to guide the snapshots towards satisfying the mass conservation equation while maintaining a limited range of velocity reconstruction errors. Compared to non-physical model, the PINN network enhanced reconstruction quality by about 28% and 29% in terms of mass conservation residual and dominant velocity component, respectively, in expense of 5% increase in the number of vectors with reconstruction error larger than the uncertainty band.

## Acknowledgements

Authors extend their sincere gratitude to Mr. Ali Shadmani for his dedicated efforts, which significantly contributed to the valuable PIV data utilized in this article.

## conflict of interest statement

The authors have no conflicts to disclose.

## Author contributions

The contributions of authors in this study are as follows:

- Maryam Soltani: Methodology; Modeling; Formal analysis; Writing – original draft.
- Ghasem Akbari: Conceptualization; Methodology; Review & editing; Supervision.
- Nader Montazerin: Conceptualization; Methodology; Review & editing; Supervision.

## Data availability statement

The data that support the findings of this study are available from the corresponding author upon reasonable request. The source codes and sample data will be included after acceptance of the article through GitHub repository.

## Appendix: Samples of reconstructed velocity fields

Figures A1 and A2 illustrate samples of reconstructed velocity fields, based on DNS and PIV data, respectively. Figure A1 has four columns, in which the first two left columns represent reconstruction of horizontal and vertical velocity components for one random DNS snapshot, based on various configurations of loss weights. The other two columns illustrate the error between target and reconstructed images. Figure A2 indicates the results of PIV data reconstruction for three random snapshots in horizontal and vertical directions, based on different weight coefficients. The last row, in both Figures A1 and A2, belongs to the baseline (non-physics-based) network.

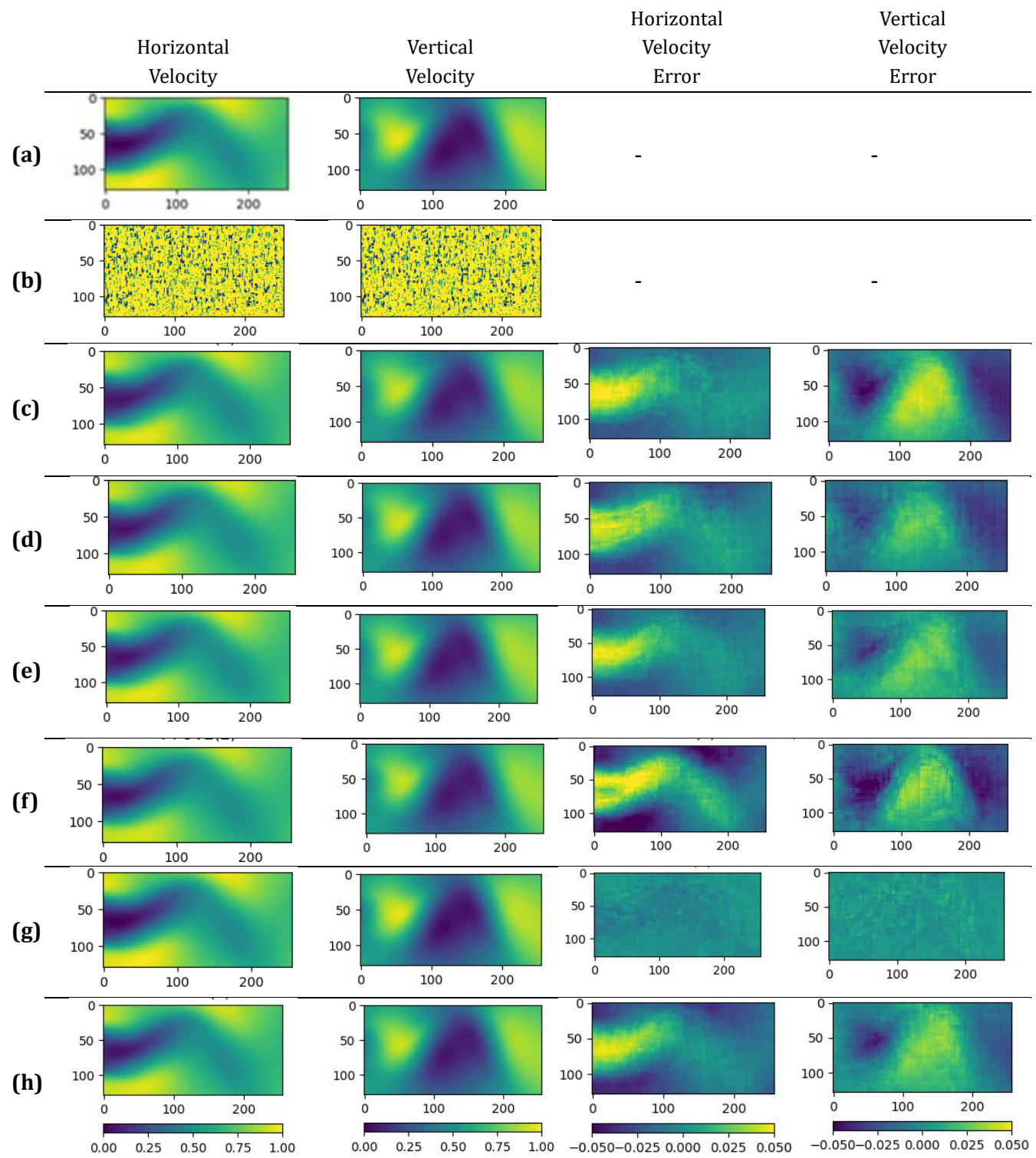


Figure A1. Samples of Reconstructed velocity field for DNS Data: a) target field; b) artificial gaps; c)  $\alpha_p = 0.1, \alpha_d = 1$ ; d)  $\alpha_p = 0.01, \alpha_d = 1$ ; e)  $\alpha_p = 1, \alpha_d = 1$ ; f)  $\alpha_p = 1, \alpha_d = 10$ ; g)  $\alpha_p = 1, \alpha_d = 100$ ; h)  $\alpha_p = 0, \alpha_d = 1$ .

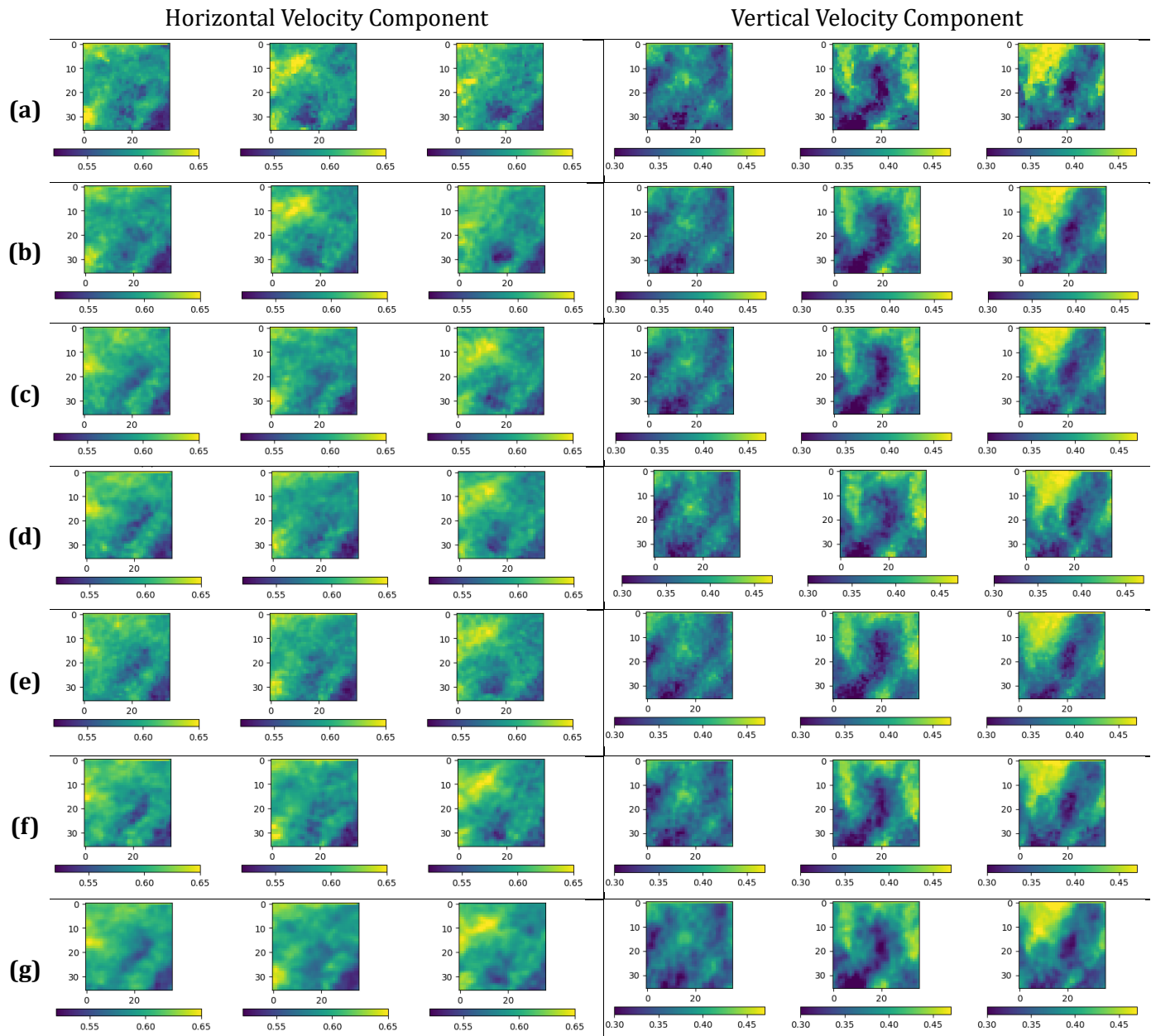


Figure A2. Three samples of reconstructed PIV Snapshots: a) Target field; b)  $\alpha_p = 0.1, \alpha_d = 1$ ; c)  $\alpha_p = 0.01, \alpha_d = 1$ ; d)  $\alpha_p = 1, \alpha_d = 1$ ; e)  $\alpha_p = 1, \alpha_d = 10$ ; f)  $\alpha_p = 1, \alpha_d = 100$ ; g)  $\alpha_p = 0, \alpha_d = 1$ .

## References

- [1] S. L. Brunton, "Applying Machine Learning to Study Fluid Mechanics," *Acta Mechanica Sinica*, vol. 37, pp. 1718–1726, Oct. 2022, [Online]. Available: <http://arxiv.org/abs/2110.02083>
- [2] R. Vinuesa and S. L. Brunton, "Enhancing Computational Fluid Dynamics with Machine Learning," *Nat Comput Sci*, vol. 2, pp. 358–366, Oct. 2021, doi: 10.1038/s43588-022-00264-7.
- [3] P. Sharma, W. T. Chung, B. Akoush, and M. Ihme, "A Review of Physics-Informed Machine Learning in Fluid Mechanics," *Energies*, vol. 16, no. 5. MDPI, Mar. 01, 2023. doi: 10.3390/en16052343.
- [4] S. G. Raben, J. J. Charonko, and P. P. Vlachos, "Adaptive gappy proper orthogonal decomposition for particle image velocimetry data reconstruction," *Meas Sci Technol*, vol. 23, no. 2, p. 025303, Feb. 2012, doi: 10.1088/0957-0233/23/2/025303.
- [5] Xin Wen, Ziyan Li, Di Peng, Wenwu Zhou, Yingzheng Liu, "Missing data recovery using data fusion of incomplete complementary data sets: A particle image velocimetry application," *Physics of Fluids*, vol. 31, no. 2, p. 025105, Feb. 2019, doi: 10.1063/1.5079896.
- [6] L. Gao *et al.*, "Reconstruction of missing data in weather radar image sequences using deep neuron networks," *Applied Sciences (Switzerland)*, vol. 11, no. 4, pp. 1–21, Feb. 2021, doi: 10.3390/app11041491.
- [7] M. Likowski, M. Smieja, L. Struski, and J. Tabor, "MisConv: Convolutional Neural Networks for Missing Data," in *2022 IEEE/CVF Winter Conference on Applications of Computer Vision (WACV)*, Los Alamitos, CA, USA: IEEE Computer Society, Jan. 2022, pp. 2917–2926. doi: 10.1109/WACV51458.2022.00297.
- [8] Q. Zhang, Q. Yuan, C. Zeng, X. Li, and Y. Wei, "Missing Data Reconstruction in Remote Sensing Image With a Unified Spatial–Temporal–Spectral Deep Convolutional Neural Network," *IEEE Transactions on Geoscience and Remote Sensing*, vol. 56, no. 8, pp. 4274–4288, 2018, doi: 10.1109/TGRS.2018.2810208.
- [9] K. Fukami, K. Fukagata, and K. Taira, "Super-resolution reconstruction of turbulent flows with machine learning," *J Fluid Mech*, vol. 870, pp. 106–120, Nov. 2019, doi: 10.1017/jfm.2019.238.
- [10] Y. Xie, E. Franz, M. Chu, and N. Thuerey, "TempoGAN: A temporally coherent, volumetric GAN for super-resolution fluid flow," *ACM Trans Graph*, vol. 37, no. 4, 2018, doi: 10.1145/3197517.3201304.
- [11] L. Yu, M. Z. Yousif, M. Zhang, S. Hoyas, R. Vinuesa, and H. C. Lim, "Three-dimensional ESRGAN for super-resolution reconstruction of turbulent flows with tricubic interpolation-

based transfer learning," *Physics of Fluids*, vol. 34, no. 12, Dec. 2022, doi: 10.1063/5.0129203.

[12] S. Oh, S. Lee, M. Son, J. Kim, and H. Ki, "Accurate prediction of the particle image velocimetry flow field and rotor thrust using deep learning," *J Fluid Mech*, vol. 939, p. A2, May 2022, doi: 10.1017/jfm.2022.135.

[13] Z. Den, Z. He, Y. Liu, and K. C. Kim, "Super-resolution reconstruction of turbulent velocity fields using a generative adversarial network-based artificial intelligence framework," *Physics of Fluids*, vol. 31, no. 12, p. 125111, Dec. 2019, doi: 10.1063/1.5127031.

[14] Bo Liu, Jiupeng Tang, Haibo Huang, and Xi-Yun Lu, "Deep learning methods for super-resolution reconstruction of turbulent flows," *Physics of Fluids*, vol. 32, no. 2, Feb. 2020.

[15] G. Akbari and N. Montazerin, "Reconstruction of particle image velocimetry data using flow-based features and validation index: A machine learning approach," *Meas Sci Technol*, vol. 33, no. 1, Jan. 2022, doi: 10.1088/1361-6501/ac2cf4.

[16] M. Raissi, P. Perdikaris, and G. E. Karniadakis, "Physics-informed neural networks: A deep learning framework for solving forward and inverse problems involving nonlinear partial differential equations," *J Comput Phys*, vol. 378, pp. 686–707, Feb. 2019, doi: 10.1016/j.jcp.2018.10.045.

[17] X. Jin, S. Cai, H. Li, and G. E. Karniadakis, "NSFnets (Navier-Stokes Flow nets): Physics-informed neural networks for the incompressible Navier-Stokes equations," *J Comput Phys*, vol. 426, Mar. 2020, doi: 10.1016/j.jcp.2020.109951.

[18] G. E. Karniadakis, I. G. Kevrekidis, L. Lu, P. Perdikaris, S. Wang, and L. Yang, "Physics-informed machine learning," *Nature Reviews Physics*, vol. 3, no. 6. Springer Nature, pp. 422–440, Jun. 01, 2021. doi: 10.1038/s42254-021-00314-5.

[19] A. Arzani, J. X. Wang, and R. M. D'Souza, "Uncovering near-wall blood flow from sparse data with physics-informed neural networks," *Physics of Fluids*, vol. 33, no. 7, Jul. 2021, doi: 10.1063/5.0055600.

[20] V. Sekar, Q. Jiang, C. Shu, and B. C. Khoo, "Accurate near wall steady flow field prediction using Physics Informed Neural Network (PINN).", 7 Apr. 2022, arXiv preprint arXiv:2204.0335.

[21] S. Cai, Z. Mao, Z. Wang, M. Yin, and G. E. Karniadakis, "Physics-informed neural networks (PINNs) for fluid mechanics: A review," *Acta Mech. Sin.* 37, pp. 1727–1738, May 2021, [Online]. Available: <http://arxiv.org/abs/2105.09506>

[22] G. Hasanuzzaman, H. Eivazi, S. Merbold, C. Egbers, and R. Vinuesa, "Enhancement of PIV measurements via physics-informed neural networks," *Meas Sci Technol*, vol. 34, no. 4, Apr. 2023, doi: 10.1088/1361-6501/aca9eb.

- [23] M. A. Calicchia, R. Mittal, J.-H. Seo, and R. Ni, "Reconstructing the pressure field around a swimming fish using a physics-informed neural network 2 3," *journal of experimental biology*, 2023, doi: 10.1101/2023.02.27.530217.
- [24] V. Kag, K. Seshasayanan, and V. Gopinath, "Physics-informed data based neural networks for two-dimensional turbulence," *Physics of Fluids*, vol. 34, no. 5, Mar. 2022, doi: 10.1063/5.0090050.
- [25] P. C. Di Leoni, K. Agarwal, T. Zaki, C. Meneveau, and J. Katz, "Reconstructing velocity and pressure from sparse noisy particle tracks using Physics-Informed Neural Networks," *Exp Fluids*, Oct. 2022, doi: 10.1007/s00348-023-03629-4.
- [26] S. Wang, Y. Teng, and P. Perdikaris, "Understanding and mitigating gradient pathologies in physics-informed neural networks," *Society for Industrial and Applied Mathematics*, vol. 43, no. 5, Jan. 2020, [Online]. Available: <http://arxiv.org/abs/2001.04536>
- [27] S. Wang, X. Yu, and P. Perdikaris, "When and why PINNs fail to train: A neural tangent kernel perspective," *J Comput Phys*, vol. 449, Jul. 2020, [Online]. Available: <http://arxiv.org/abs/2007.14527>
- [28] L. McClenny and U. Braga-Neto, "Self-Adaptive Physics-Informed Neural Networks using a Soft Attention Mechanism," *J Comput Phys*, vol. 474, Sep. 2020, [Online]. Available: <http://arxiv.org/abs/2009.04544>
- [29] H. Eivazi and R. Vinuesa, "Physics-informed deep-learning applications to experimental fluid mechanics," Mar. 2022, [Online]. Available: <http://arxiv.org/abs/2203.15402>
- [30] S. Cai, Z. Wang, F. Fuest, Y.-J. Jeon, C. Gray, and G. E. Karniadakis, "Flow over an espresso cup: Inferring 3D velocity and pressure fields from tomographic background oriented schlieren videos via physics-informed neural networks," *J Fluid Mech*, vol. 915, Mar. 2021, doi: 10.1017/jfm.2021.135.
- [31] H. Wang, Y. Liu, and S. Wang, "Dense velocity reconstruction from particle image velocimetry/particle tracking velocimetry using a physics-informed neural network," *Physics of Fluids*, vol. 34, no. 1, Jan. 2022, doi: 10.1063/5.0078143.
- [32] G. Akbari, N. Montazerin, and M. Akbarizadeh, "Stereoscopic particle image velocimetry of the flow field in the rotor exit region of a forward-blade centrifugal turbomachine," *Proceedings of the Institution of Mechanical Engineers, Part A: Journal of Power and Energy*, vol. 226, no. 2, pp. 163–181, 2012, doi: 10.1177/0957650911430285.
- [33] "1997 BS848, Fans for general purposes, part 1: methods for testing performances (London: British Standard Institution)".
- [34] J. Taylor, W. Wang, B. Bala, and T. Bednarz, "Optimizing the optimizer for data driven deep neural networks and physics informed neural networks," May 2022, [Online]. Available: <http://arxiv.org/abs/2205.07430>

- [35] E. McGowan, V. Gawade, and W. (Grace) Guo, "A Physics-Informed Convolutional Neural Network with Custom Loss Functions for Porosity Prediction in Laser Metal Deposition," *Sensors*, vol. 22, no. 2, p. 494, Jan. 2022, doi: 10.3390/s22020494.
- [36] H. Gao, L. Sun, and J.-X. Wang, "Super-resolution and denoising of fluid flow using physics-informed convolutional neural networks without high-resolution labels," *Physics of Fluids*, vol. 33, no. 7, Nov. 2021, doi: 10.1063/5.0054312.
- [37] P.-H. Chiu, J. Cheng Wong, C. Ooi, M. H. Dao, and Y.-S. Ong, "CAN-PINN: A Fast Physics-Informed Neural Network Based on Coupled-Automatic-Numerical Differentiation Method."
- [38] Z. Xiang, W. Peng, X. Liu, and W. Yao, "Self-adaptive loss balanced Physics-informed neural networks," *Neurocomputing*, vol. 496, pp. 11–34, 2022, doi: <https://doi.org/10.1016/j.neucom.2022.05.015>.
- [39] J. N. Kutz, S. L. (Steven L. Brunton, B. W. Brunton, and J. L. Procor, *Dynamic mode decomposition : data-driven modeling of complex systems*.
- [40] G. Akbari and N. Montazerin, "On the role of anisotropic turbomachinery flow structures in inter-scale turbulence energy flux as deduced from SPIV measurements," *Journal of Turbulence*, vol. 14, no. 11, pp. 44–70, Nov. 2013, doi: 10.1080/14685248.2013.861073.